Porous nitrogen-doped carbon supported MoO$_2$/Mo$_2$C hybrid catalyst for efficient oxidative coupling of primary amines to imines

Wen-Ting Chen[1,2] · Song Han[1] · Zhi-Hong Dai[1] · Yu-Xuan Fu[1] · Ming-Shuai Sun[1] · Zhang-Min Li[1] · Yan Zhou[1] · Duan-Jian Tao[1]

Abstract

A MoO$_2$/Mo$_2$C hybrid catalyst supported on N-doped carbon (Mo$_2$C/MoO$_2$@NC) was successfully prepared, which is featured with moderate mesoporosity, uniform metallic nanoparticles, and rich oxygen-vacancies. It showed excellent efficiency (99% imine yield) and good reusability for oxidative self-coupling of benzylamine to *N*-benzylbenzaldimine under mild conditions (85 °C, 3 h, 1 bar O$_2$). In addition, the catalyst Mo$_2$C/MoO$_2$@NC also exhibited a universal applicability for oxidative coupling of other primary amines to imines with impressive conversion and satisfying target product selectivity. This method provides an efficient and environment friendly strategy for catalytic synthesis of complex imines from primary amines.

Keywords Amines · Imines · Oxidative self-coupling · Molybdenum carbide · Oxygen vacancy

1 Introduction

Transition metals carbides are formed by dissolving C in melts of metals [1]. They exhibit high hydrogen adsorptivity and electrical conductivity, which is good for several catalytic dehydrogenation reactions [2]. As a representative candidate, molybdenum carbide (Mo$_2$C) displays Pt-like features and thereby shows good performance in dehydrogenation, hydrogen evolution reaction, etc. [3–6]. However, many important valuable fine-chemicals are often synthesized through a multiple complex reaction involving both dehydrogenation and oxidation. The previous reported Mo$_2$C-based catalysts could hard to efficiently catalyze those multiple reactions because of their poor oxidizability. Therefore, it is demanded and conceived to fabricate Mo$_2$C-based hybrid catalyst with boosting both dehydrogenization and oxidizability.

It is indicated that the oxygen defects in metal oxide are as a crucial factor for boosting the oxidation properties. So far, various metal oxides such as TiO$_2$ [7, 8], CeO$_2$ [9, 10], MoO$_x$ [11–13], WO$_2$ [14] with enriched oxygen vacancies have been prepared and served as efficient catalysts for oxidation reactions. For example, by making use of oxygen vacancy defects on the surface of metal oxides, the excellent catalytic performance of Cu-doped CeO$_2$ nanocrystals was achieved for synthesis of imines [10]. The CeO$_2$–MoO$_3$/SiO$_2$ hybrid material was also reported to serve as a good catalyst for oxidation of benzylamines to synthesis of *N*-benzylbenzaldimines because of their abundant oxygen vacancies [13]. Therefore, in light of the nature of abundant oxygen vacancies in MoO$_2$, fabricating the MoO$_2$/Mo$_2$C hybrid material is an effective method of boosting both dehydrogenization and oxidizability.

Imines are of great importance in the synthesis of dyes, agrochemicals, fungicides, pharmaceuticals, and materials [15, 16]. Recently, the oxidative self-coupling of primary amines has been considered to be one of the most promising methodologies for preparation of imines [17]. For achieving efficient transformation, the qualified catalyst must have the

✉ Yan Zhou
anitachow@jxnu.edu.cn

✉ Duan-Jian Tao
djtao@jxnu.edu.cn

1 National Engineering Research Center for Carbohydrate Synthesis, Key Laboratory of Fluorine and Silicon for Energy Materials and Chemistry of Ministry of Education, College of Chemistry and Chemical Engineering, Jiangxi Normal University, Nanchang 330022, China

2 School of Chemical Engineering, Guizhou Institute of Technology, Guiyang 550003, China

comprehensive ability of both dehydrogenization and oxidizability. The key step is that to activate the oxidant (such as molecular O_2) and dehydrogenate primary amine into an NH-imine intermediate. This allows us to realize that the MoO_2/Mo_2C hybrid material have potential to be a promising catalyst for the oxidative coupling of primary amines.

Herein, a nitrogen-doped carbon (NC) supported MoO_2/Mo_2C hybrid material was designed and prepared. The as-prepared Mo_2C/MoO_2@NC catalyst was employed for oxidative self-coupling of benzylamine to *N*-benzylbenzaldimine with good yield. A series of characterizations further indicated that the catalyst Mo_2C/MoO_2@NC exhibited the characteristics of abundant mesoporosity, well-shaped nanoparticles, and oxygen-rich vacancies, which accounts for the excellent catalytic performance. In addition, the applicability and reusability of Mo_2C/MoO_2@NC were also studied.

2 Experimental section

2.1 Materials

Molybdic acid (85%), urea (99%), benzylamine (99%), cellulose (98%), and 2,2,6,6-tetramethylpiperidinooxy (TEMPO) were obtained from Shanghai Macklin Co., Ltd. Butylated hydroxytoluene (94%), phenylethylamine (96%), *p*-methylbenzylamine (98%), *p*-fluorphenimide (99%), *p*-chlorobenzene methylamine (95%), and *p*-bromobenzylamine (96%) purchased from Shanghai Aladdin Co., Ltd. Other reagents were used without any purification.

2.2 *Preparation of g-C₃N₄*

The synthesis method of g-C_3N_4 was according to the reported previous literature [18]. For example, 5.0 g of urea was added in a covered ceramic crucible and put into a tube furnace. Then, a heating program of furnace was set as 550 °C for 2 h with a rate of 2.5 °C/min. After completion of annealing, the g-C_3N_4 sample was produced as a pale-yellow solid.

2.3 Preparation of molybdenum hybrid catalysts

The molybdenum hybrid catalysts were prepared via a combination of ball grinding and high annealing. Typically, g-C_3N_4 (1.5 g), molybdic acid (0.3 g), and cellulose (1.5 g) were added into an agate mortar. The solid mixture was then homogeneously grinded by ball-milling for 2 h. The resultant solid powder was heated at 700 °C for 2 h with a heating speed of 5 °C/min using argon flow. After that, the Mo_2C/MoO_2@NC sample was obtained. For comparison, the other two MoO_2/Mo_2C@NC-600 and MoO_2/Mo_2C@NC-800

catalysts were also prepared at the carbonization temperature of 600 and 800 °C, respectively. Besides, the MoO_2@C catalyst was prepared with the above procedures except for using the precursor g-C_3N_4. The Mo_2C@NC catalyst was also prepared with the above procedures by using molybdic acid (0.3 g), g-C_3N_4 (2 g), and cellulose (1 g). Commercial Mo_2C powder, commercial MoO_2 powder, and activated carbon were mixed by mechanical grinding and annealing at 700 °C for 2 h to obtain the Mo_2C-MoO_2/AC sample.

2.4 Characterization

The crystalline structure of the sample was analyzed using X-ray diffraction (XRD, Rigaku RINT-2200) with a Cu-Kα source. N_2 adsorption–desorption isotherms were measured on a Micromeritics TriStar II 3020 instrument to calculate the Brunauer–Emmett–Teller (BET) specific surface areas and obtain the pore size distribution from the analysis of Barrett-Joyner-Halenda (BJH). Scanning electron microscope (SEM), transmission electron microscopy (TEM), and high-resolution transmission electron microscopy (HRTEM) images were obtained using HITACHI S3400N and JEOL JEM-2100 instruments, respectively. The hydrogen temperature-programmed reduction (H_2-TPR) tests were carried out by Micromeritics Autochem II 2920 with the temperature increased from 100 °C to 600 °C. X-ray photoelectron spectroscopy (XPS) spectra were acquired using an AXIS Supra spectrometer with Al Kα as the excitation source. Electron paramagnetic resonance (EPR) spectra was conducted on a EMXplus-9.5/12 spectrometer (Bruker) at room temperature.

2.5 Catalytic reaction

The reaction of benzylamine to *N*-benzylbenzaldimine was performed in a 30 mL reactor. Typically, benzylamine (1 mmol), Mo_2C/MoO_2@NC catalyst (50 mg), and acetonitrile (5 mL) were gradually charged into the reactor. Then the reactor was heated to 85 °C for 3 h with 1 bar O_2. After the completion of reaction, the Mo_2C/MoO_2@NC catalyst was filtered. The recycled catalyst was washed with ethanol and dried for 5 h in a vacuum oven at 60 °C for a next run. The determination of reaction products was listed in the supplementary material.

3 Results and discussion

3.1 Characterization results

Figure 1 shows Raman spectra of D band at 1330 cm^{-1} and G band at 1605 cm^{-1} [19] in these three MoO_2@C, Mo_2C/MoO_2@NC, and Mo_2C@NC samples. This suggests that
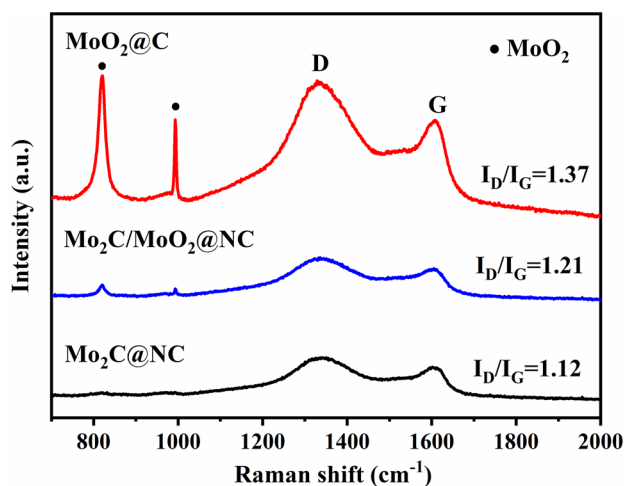
Fig. 1 Raman spectra of MoO$_2$@C, Mo$_2$C/MoO$_2$@NC, and Mo$_2$C@NC samples
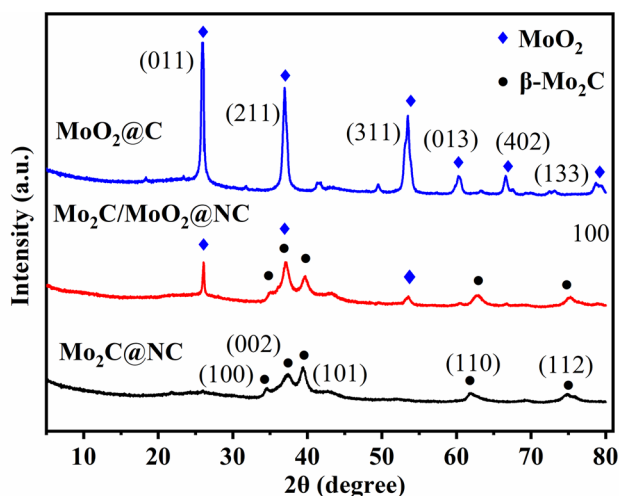
Fig. 2 XRD patterns of MoO$_2$@C, Mo$_2$C/MoO$_2$@NC and Mo$_2$C@NC samples
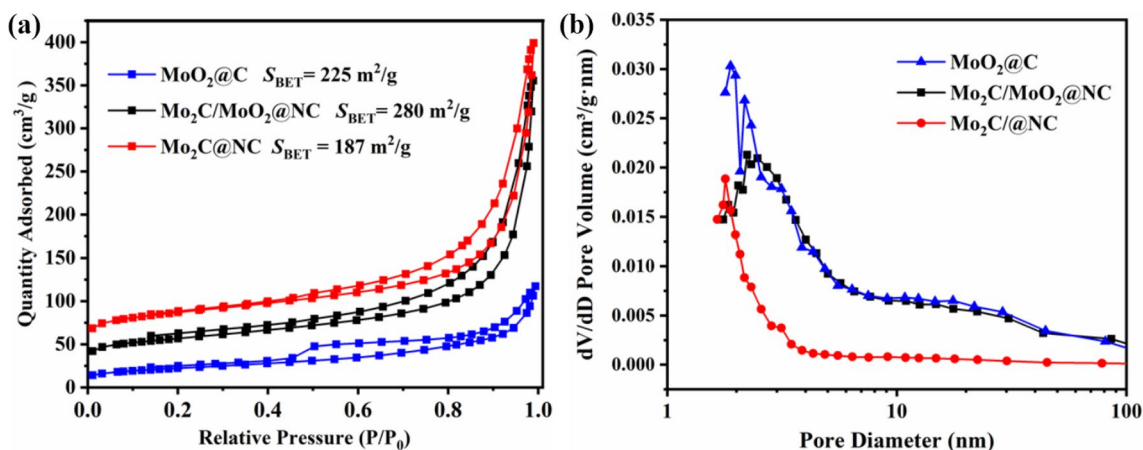
the support carbon frameworks were formed in these three samples after a high-temperature calcination. Moreover, the intensity ratio of the D band to the G band, named I$_D$/I$_G$, can reveal the defects of carbon frameworks. Mo$_2$C/MoO$_2$@NC exhibited a I$_D$/I$_G$ ratio of 1.21, indicating the presence of abundant defects. In addition, the characteristic peaks at 820 and 996 cm^{-1} were found in Mo$_2$C/MoO$_2$@NC and MoO$_2$@C, which is ascribed to the stretching vibration of Mo − O bond [20].

Figure 2 shows the XRD patterns of the Mo$_2$C/MoO$_2$@ NC, MoO$_2$@C, Mo$_2$C@NC samples. First, three intensified peaks of MoO$_2$@C sample were found at 26.0°, 37.0°, and 53.6°, which corresponds to the (011), (211), (311) crystal plane of monoclinic MoO$_2$ (JCPDS No. 78-1072) [12, 21]. Meanwhile, five characteristic peaks of Mo$_2$C@NC sample were observed at 34.4°, 37.9°, 39.5°, 61.7°, and 74.7°, which is assigned to the (100), (002), (101), (110), and (112) crystal planes of β-Mo$_2$C (JCPDS No. 35-0787) [4, 22]. For comparison, all the above characteristic diffraction peaks of both Mo$_2$C and MoO$_2$ were simultaneously found in the Mo$_2$C/MoO$_2$@NC sample, demonstrating the successful formation of hybrid MoO$_2$/Mo$_2$C supported on carbon material. Setting an appropriate mass ratio of those three precursors, the Mo$_2$C and MoO$_2$ nanoparticles can be formed and co-existed in the Mo$_2$C/MoO$_2$@NC hybrid material.

The results of N$_2$ adsorption/desorption isotherms and pore size of molybdenum hybrid samples were shown in Fig. 3. The MoO$_2$@C sample exhibited IV-type isotherms with a H4 hysteresis loop (Fig. 3a), while the Mo$_2$C/MoO$_2$@ NC and Mo$_2$C@NC samples showed IV-type isotherms with H3 hysteresis loops [23]. This result demonstrates the presence of abundant mesopores in all of these three samples. As shown in Fig. 3b, the Mo$_2$C/MoO$_2$@NC had a high BET surface area of 280 m^2/g with a pore size of 2.3 nm from the BJH analysis, which is much larger than MoO$_2$@C (225 m^2/g, 1.9 nm) and Mo$_2$C@NC (187 m^2/g,

Fig. 3 N$_2$ adsorption–desorption isotherms and pore size distribution of MoO$_2$@C, Mo$_2$C/MoO$_2$@NC and Mo$_2$C@NC samples at − 196 °C

1.8 nm). Apparently, the Mo$_2$C/MoO$_2$@NC sample had a predominance of larger surface area, which can expose more sufficient active sites for reaction.

The SEM, TEM, and HRTEM images of molybdenum hybrid samples were shown in Fig. 4. It can be seen from SEM images that the Mo$_2$C/MoO$_2$@NC sample possessed curly and wrinkled porous layered nanostructures. The TEM images of Mo$_2$C/MoO$_2$@NC further showed the high dispersion and encapsulation of the Mo$_2$C/MoO$_2$ dots (average size of 3.2 nm) into the N-doped carbon framework. Moreover, the Mo$_2$C crystal plane spacing was observed to be 0.24 nm, which is assigned to the (002) crystal plane of β-Mo$_2$C. The (011) d-spacing of MoO$_2$ nanoparticles was also measured as 0.34 nm from the HRTEM images. These results again validate the formation of crystallized β-Mo$_2$C and MoO$_2$ nanoparticles in the Mo$_2$C/MoO$_2$@NC hybrid material, which is accordance with the XRD and Raman measurements.

As shown in Figure S1 in supplementary material, the H$_2$-TPR profile of Mo$_2$C/MoO$_2$@NC had a relatively sharp shoulder peak at 358 °C. This implies the uniform Mo$_2$C/MoO$_2$ nanoparticles size and orderly morphology of Mo$_2$C/MoO$_2$@NC [24]. For comparison, no obvious peak was found in the H$_2$-TPR profile of Mo$_2$O@C. A broad shoulder peak located at 312 °C was observed for Mo$_2$C@NC. It is believed that a stronger interaction between molybdenum species and carbon support would verify in the Mo$_2$C/MoO$_2$@NC sample.

The full-scan XPS spectra of the MoO$_2$@C, Mo$_2$C/MoO$_2$@NC, and Mo$_2$C@NC samples was shown in Figure S2 in supplementary material. It is demonstrated that all these three samples included the Mo, C, N, and O elements. The XPS spectra of Mo 3d was further deconvoluted into three different Mo species (Fig. 5), assigning to Mo^{6+} at 232.7 ± 0.1 eV, Mo^{4+} at 230.1 ± 0.6 eV, and Mo^{2+} at 228.8 ± 0.3 eV, respectively [25]. Notably, the binding energies of Mo^{2+} in Mo$_2$C/MoO$_2$@NC and Mo$_2$C@NC (228.8 eV) were slightly lower than that in MoO$_2$@C (229.1 eV) without containing N element. This shows that the N element is beneficial for formation of more low-valence Mo^{2+} species, which would modulate the catalytic activities of these molybdenum hybrid materials [26]. Regarding the N 1 s spectra of Mo$_2$C/MoO$_2$@NC and Mo$_2$C@NC (Figure S3, supplementary material), three distinct peaks were observer at 401.6, 400.8, and 398.6 eV, which belongs to graphitic-N, pyrrolic-N, and
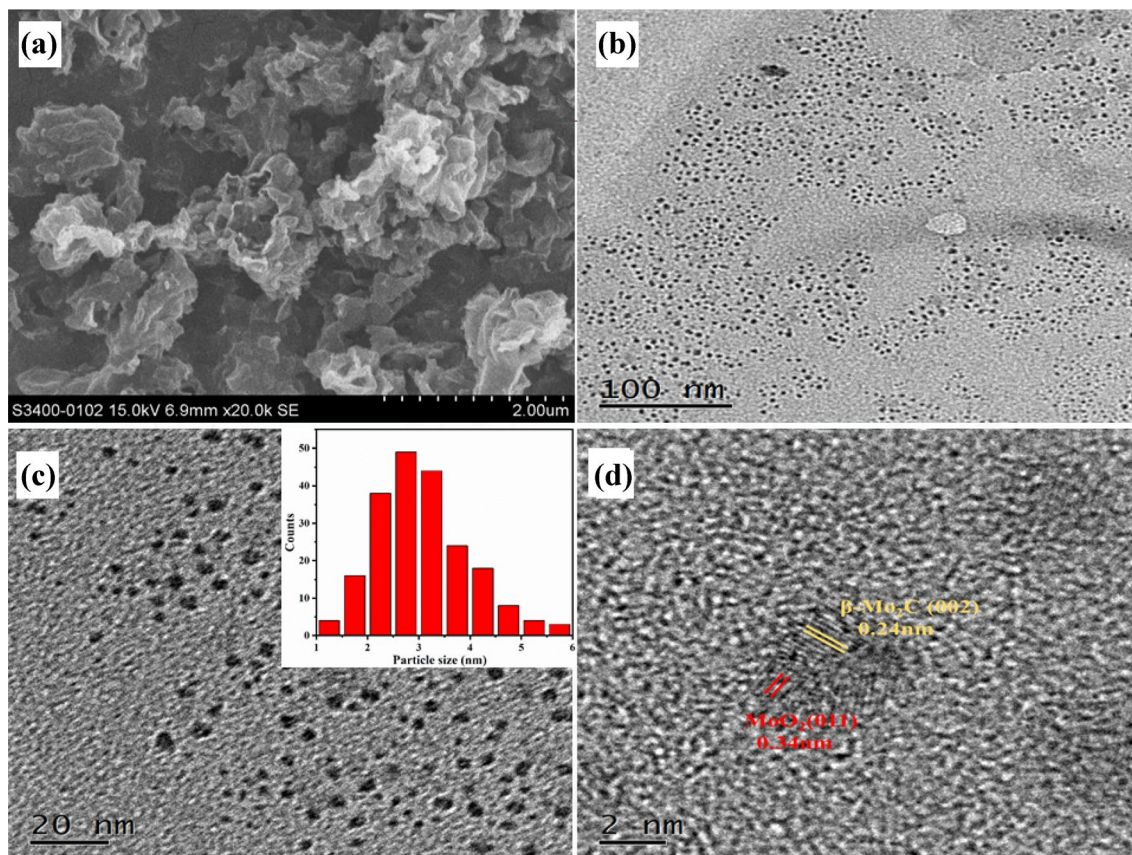

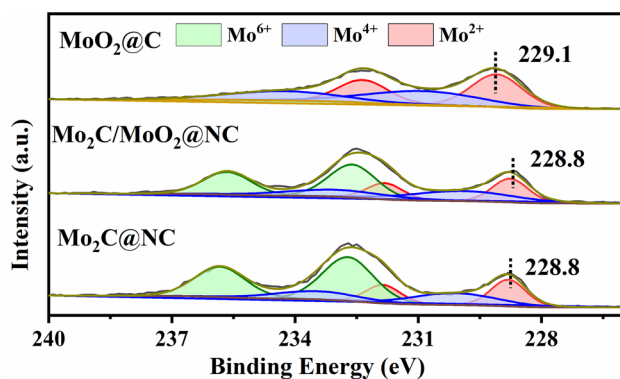**Fig. 4** SEM, TEM, and HRTEM images of Mo$_2$C/MoO$_2$@NC (inset: nanoparticle size distribution)

Fig. 5 XPS profiles of Mo 3d in the MoO_2@C, Mo_2C/MoO_2@NC, and Mo_2C@NC samples

pyridinic-N, respectively. The percentage of pyridinic N in Mo_2C/MoO_2@NC was higher than that in Mo_2C@NC, and the more content of pyridine-N can improve the catalytic performance in many oxidation reactions [27].

In addition, the XPS spectra of O 1 s in the MoO_2@C, Mo_2C/MoO_2@NC, and Mo_2C@NC materials was shown in Figure S4 in supplementary material. The deconvoluted peaks at ~530.3 eV and ~532.1 eV was assigned to the lattice oxygen and the surface adsorbed oxygen, respectively. The content of surface adsorption oxygen in Mo_2C/MoO_2@NC was obviously higher than that in MoO_2@C and Mo_2C@NC. That is to say, it is more likely for Mo_2C/MoO_2@NC to own oxygen vacancies owing to its more proportional surface absorbed oxygen species [28]. To directly confirm the existence of oxygen vacancies, the MoO_2@C, Mo_2C/MoO_2@NC, and Mo_2C@NC samples were characterized by EPR spectroscopy. It is seen from Fig. 6 that Mo_2C/MoO_2@NC exhibited an obvious EPR signal at g = 2.003, verifying
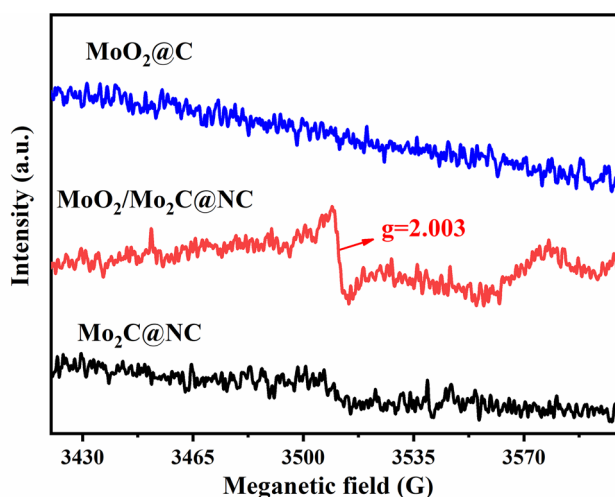
the presence of oxygen vacancies in Mo_2C/MoO_2@NC [29]. For comparison, no signal for oxygen vacancies was detected in Mo_2C@NC and MoO_2@C. Therefore, it is indicated that N-doped carbon supported MoO_2/Mo_2C hybrid material with incorporated rich oxygen vacancies was successfully prepared and characterized.

3.2 Catalytic performance

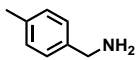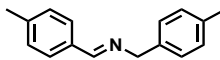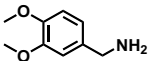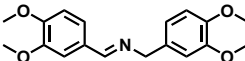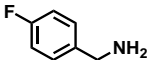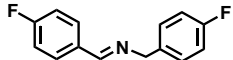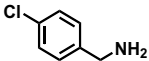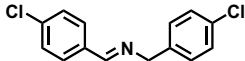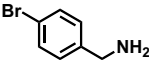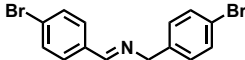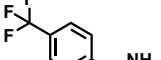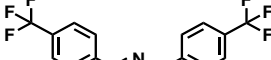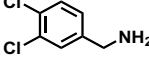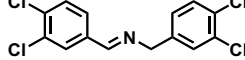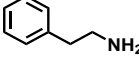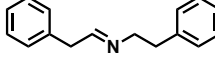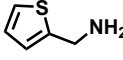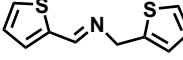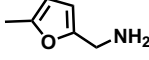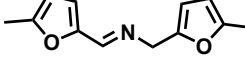The as-prepared molybdenum hybrid catalysts were employed for oxidative self-coupling of benzylamine to N-benzylbenzaldimine (Table 1). An outstanding catalytic performance with 99% benzylamine conversion and 99% N-benzylbenzaldimine yield was achieved on Mo_2C/MoO_2@NC. However, Mo_2C@NC and MoO_2@C only gave 66% and 32% N-benzylbenzaldimine yields, respectively (Table 1, entries 1, 2). From entries 4 and 5 in Table 1, it can be seen that the coupling reaction of benzylamine could not proceed without catalyst and just a negligible conversion (3%) was determined in the presence of bare support (NC). A single molybdenum compound (Mo_2C or MoO_2) could not catalyze this reaction efficiently as shown in entries 6 and 7 (Table 1). Above comparison indicates that there are positive synergistic effects between Mo_2C, MoO_2 and NC carrier, which have ensured the excellent catalytic performance of Mo_2C/MoO_2@NC. Moreover, the optimization of the coupling reaction conditions using the MoO_2/Mo_2C@NC catalyst was systematically studied. It is found that strong polar solvents were beneficial to the oxidative self-coupling reaction of

Table 1 Oxidative self-coupling of benzylamine to N-benzylbenzaldimine using different catalysts
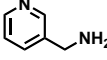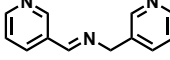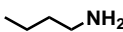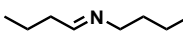

Entry	Catalyst	Conversion (%)	Yield (%)
1	MoO_2/Mo_2C@NC	99	99
2	Mo_2C@NC	66	66
3	MoO_2@C	32	32
4	–	0	0
5	NC	3	3
6	Commercial Mo_2C	6	6
7	Commercial MoO_2	3	3
8	Mo_2C-MoO_2/AC	20	15
9	MoO_2/Mo_2C@NC-600	57	55
10	MoO_2/Mo_2C@NC-800	17	13
11[a]	MoO_2/Mo_2C@NC	0	0

Reaction conditions: benzylamine (1 mmol), catalyst (50 mg), acetonitrile (5 mL), 1 bar O_2, 85 °C, 600 rpm, 3 h. [a]1 bar N_2

Fig. 6 EPR spectra of MoO_2@C, Mo_2C/MoO_2@NC and Mo_2C@NC samples at 25 °C

Table 2 Oxidative self-coupling of different primary amines using the MoO$_2$/Mo$_2$C@NC catalyst

Entry	Substrate	Product	Conversion	Yield
1			99%	99%
2			95%	90%
3			99%	99%
4			99%	99%
5			99%	99%
6			99%	99%
7			99%	99%
8			99%	99%
9			99%	99%
10			99%	99%
11			82%	82%
12			20%	20%

Reaction conditions: substrate (1 mmol), catalyst (0.05 g), acetonitrile (5 mL), 1 bar O$_2$, 85 °C, 3 h

benzylamine (Figure S5, supplementary material). Acetonitrile was selected as the preferred solvent in subsequent studies of other reaction parameters. After screening the effect of reaction temperature and time, the highest *N*-benzylbenzaldimine yield of 99% could be obtained in acetonitrile at the optimized condition of 85 °C and 3 h (Figures S6, S7, supplementary material).

For further comparison, the reference catalysts Mo$_2$C/MoO$_2$@NC-600, Mo$_2$C/MoO$_2$@NC-800, and Mo$_2$C-MoO$_2$/AC were tested for synthesis of *N*-benzylbenzyldimine (Table 1, entries 8–10). These three catalysts all exhibited below 60% *N*-benzylbenzyldimine yield, showing that the NC support and carbonization temperature are key roles for improving the yield of *N*-benzylbenzyldimine. It is because that the surface of NC carrier could highly disperse the
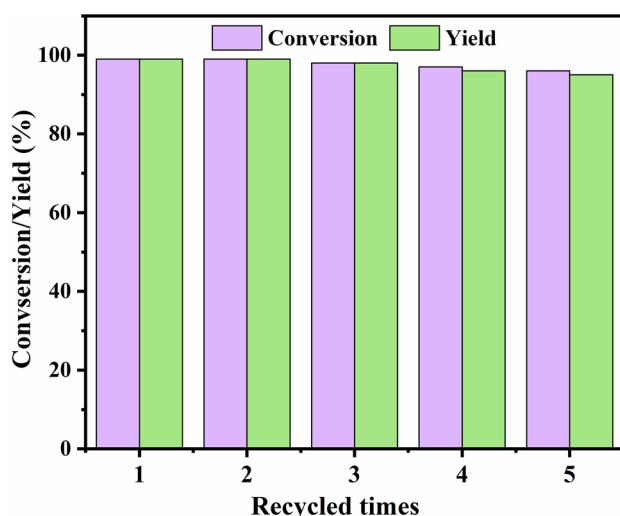
Fig. 7 Reusability of Mo$_2$C/MoO$_2$@NC in oxidative self-coupling of benzylamine

heterojunction nanoparticles of β-Mo$_2$C and MoO$_2$ in Mo$_2$C/MoO$_2$@NC. Mo$_2$C/MoO$_2$@NC also possessed the highest specific surface area with 280 m^2/g compared with Mo$_2$C/MoO$_2$@NC-600 and Mo$_2$C/MoO$_2$@NC-800 (Figure S8, supplementary material), which provides more active sites to achieve such excellence performance in oxidative self-coupling of benzylamine.

To investigate the possible important role of oxygen vacancies on Mo$_2$C/MoO$_2$@NC catalyst in this reaction, further experiments were conducted. After the reactant gas O$_2$ (1 bar) was replaced by N$_2$ (1 bar), no benzylamine conversion was detected (Table 1, entry 11). This proves the necessity for oxygen to participate in benzylamine self-coupling reaction. Furthermore, amine overoxidation products such as ketones and aldehydes were not found by GC–MS. Therefore, it is speculated that Mo$_2$C would dehydrogenate NH$_2$-amine into an NH-imine intermediate, as well as rich oxygen-vacancies in the MoO$_2$ nanoparticles would activate the oxidant molecular O$_2$, which readily enables the NH-imine intermediate to lose NH$_3$ and gives the imine coupling product [30, 31]. Finally, the catalytic performance of MoO$_2$/Mo$_2$C@NC with previous studies was compared and listed in Table S1 (supplementary material). It can be observed that in order to obtain excellent conversions of benzylamine, the currently available catalysts suffered from the drawbacks such as very long reaction time and noble metal catalysts (e.g., 12–24 h, Au/Pd) [32–36]. On the contrary, by using MoO$_2$/Mo$_2$C@NC as catalyst, the reaction time could significantly be reduced to 3 h with a yield of 99% *N*-benzylbenzaldimine.

3.3 *Applicability and reusability of* MoO$_2$/Mo$_2$C@NC

The applicability of MoO$_2$/Mo$_2$C@NC was examined for catalyzing oxidative coupling of other primary amines. The results are listed in Table 2. All the structures of imines products were confirmed by GC–MS and shown in Figure S9 (supplementary material). It is indicated that various benzylamines bearing electron-withdrawing or electron-donating groups were produced to homologous substituted imines with good to excellent yields (Table 2, entries 1–7). Notably, the selective oxidative self-coupling of 2-phenylethylamine, 2-thiophenemethylamine, 5-methyl-2-furanmethanamine, and 3-(aminomethyl) pyridine could be also efficiently converted into corresponding imines with excellent activity and satisfying selectivity (Table 2, entries 8–11). However, it is indicated that the yield of *N*-butylidenebutylamine was only 20% (Table 2, entry 12). This result shows that MoO$_2$/Mo$_2$C@NC catalyst could not efficiently catalyze the oxidative self-coupling of alkyl amines.

The reusability of MoO$_2$/Mo$_2$C@NC catalyst were studied at least five successive cycles. The results are shown in Fig. 7. There is no significant decrease in benzylamine conversion and imine yield, indicating good recyclability of MoO$_2$/Mo$_2$C@NC. Moreover, it is found that both the reused and fresh catalysts showed well-preserved XRD diffraction peaks of MoO$_2$ and Mo$_2$C nanoparticles (Figure S10, supplementary material). TEM images of regenerated MoO$_2$/Mo$_2$C@NC catalyst (Figure S11, supplementary material) further demonstrated that the catalyst had no obvious change in morphology, particle size and distribution after used for up to 5 cycles. The atomic emission spectroscopy was also employed to check whether there existed the homogeneous Mo species after leaching the catalyst. It is found that trace of Mo was detected in the liquid solution. All these results show that the MoO$_2$/Mo$_2$C@NC catalyst has wonderful stability for application in oxidative self-coupling of primary amines.

4 Conclusions

A heterostructure MoO$_2$/Mo$_2$C@NC catalyst was successfully prepared and showed good activity and selectivity in the oxidative self-coupling reaction of primary amines to imines under the mildest reaction conditions, which beyond most of the reported catalysts. Highly distorted Mo$_2$C/MoO$_2$ nanoparticles supported on NC surface contribute abundant active oxygen vacancies that can effectively activate O$_2$ and achieve high selectivity in oxidative self-coupling of primary amines. This work thus triggers a more efficient and

relatively environmental approach for synthesis of complex imines via the oxidative self-coupling reaction.

Author contributions W-TC: Investigation, Writing-original draft, Data curation.SH: Methodology, Investigation.Z-HD: Methodology, Investigation.Y-XF: Methodology, Investigation.M-SS: Methodology, Investigation, Writing-review & editing.Z-ML: Funding acquisition, Methodology, Writing-review & editing.YZ: Supervision, Conceptualization, Resources, Writing-review & editing.D-JT: Supervision, Conceptualization, Funding acquisition, Resources, Writing-review & editing.

Declarations

Competing interests The authors declare no Competing interests.

References

1. J.G. Chen, Chem. Rev. **96**(4), 1477–1498 (1996)
2. N. Ji, T. Zhang, M. Zheng, A. Wang, H. Wang, X. Wang, J.G. Chen, Angew. Chem. Int. Ed. **47**(44), 8510–8513 (2008)
3. Q. Gao, W. Zhang, Z. Shi, L. Yang, Y. Tang, Adv. Mater. **31**(2), 1802880 (2019)
4. Z. Li, C. Chen, E. Zhan, N. Ta, Y. Li, W. Shen, Chem. Commun. **50**(34), 4469–4471 (2014)
5. E. Gomez, B. Yan, S. Kattel, J.G. Chen, Nat. Rev. Chem. **3**(11), 638–649 (2019)
6. H. Sun, G. Li, J. Luo, M. Rao, Z. Peng, T. Jiang, Mater. Des. **193**, 108803 (2020)
7. F.E. Kühn, A.M. Santos, M. Abrantes, Chem. Rev. **106**(6), 2455–2475 (2006)
8. Y. Zhou, Y. Chai, X. Li, Z. Wu, J. Lin, Y. Han, L. Li, H. Qi, Y. Gu, L. Kang, X. Wang, ACS Catal. **11**(24), 15223–15233 (2021)
9. R. Jana, C. Chowdhury, S. Malik, A. Datta, ACS Appl. Energy Mater. **2**(8), 5613–5621 (2019)
10. X. Huang, G. Lu, K. Zhang, J. Liu, H. Zhang, Z. Guo, J. Tao, Appl. Surf. Sci. **514**, 145948 (2020)
11. J. Xu, C. Zhang, H. Liu, J. Sun, R. Xie, Y. Qiu, F. Lü, Y. Liu, L. Zhuo, X. Liu, J. Luo, Nano Energy **70**, 104529 (2020)
12. X. Li, J. Yu, J. Jia, A. Wang, L. Zhao, T. Xiong, H. Liu, W. Zhou, Nano Energy **62**, 127–135 (2019)
13. B. Govinda Rao, P. Sudarsanam, A. Rangaswamy, B.M. Reddy, Catal. Lett. **145**(7), 1436–1445 (2015)
14. H. Tian, X. Cui, L. Zeng, L. Su, Y. Song, J. Shi, J. Mater. Chem. A **7**(11), 6285–6293 (2019)
15. C.P. Dong, Y. Higashiura, K. Marui, S. Kumazawa, A. Nomoto, M. Ueshima, A. Ogawa, ACS Omega **1**(5), 799–807 (2016)
16. L. Peng, H.G. Baldovi, A. Dhakshinamoorthy, A. Primo, H. Garcia, ACS Omega **7**(13), 11092–11100 (2022)
17. J.C. Espinosa, M. Álvaro, A. Dhakshinamoorthy, S. Navalón, H. García, ACS Sustain. Chem. Eng. **7**(19), 15948–15956 (2019)
18. H. Ji, T. Fei, L. Zhang, J. Yan, Y. Fan, J. Huang, Y. Song, Y. Man, H. Tang, H. Xu, H. Li, Appl. Surf. Sci. **457**, 1142–1150 (2018)
19. X. Liu, Y. Zhou, C.L. Wang, Y. Liu, D.J. Tao, Chem. Eng. J. **427**, 130878 (2022)
20. H. Yan, Y. Xie, Y. Jiao, A. Wu, C. Tian, X. Zhang, L. Wang, H. Fu, Adv. Mater. **30**(2), 1704156 (2018)
21. P. Phalswal, P.K. Khanna, Mater. Lett. **302**, 130445 (2021)
22. J. Jia, T. Xiong, L. Zhao, F. Wang, H. Liu, R. Hu, J. Zhou, W. Zhou, S. Chen, ACS Nano **11**(12), 12509–12518 (2017)
23. X. Zhao, Y. Zhou, K. Huang, C. Li, D.J. Tao, ACS Sustainable Chem. Eng. **7**(2), 1901–1908 (2018)
24. X. Tang, B. Zhang, Y. Li, Y. Xu, Q. Xin, W. Shen, Catal. Lett. **97**(3), 163–169 (2004)
25. W. Cui, N. Cheng, Q. Liu, C. Ge, A.M. Asiri, X. Sun, ACS Catal. **4**(8), 2658–2661 (2014)
26. L. Ma, P. Chen, G. Zhang, L. Wang, F. Tang, X. Zhao, J. Wang, J. Huang, Y.-N. Liu, ChemCatChem **13**(14), 3283–3289 (2021)
27. X. Zhao, Y. Zhou, A.L. Jin, K. Huang, F. Liu, D.J. Tao, New J. Chem. **42**(19), 15871–15878 (2018)
28. T. Li, J. He, B. Peña, C.P. Berlinguette, Angew. Chem. Int. Ed. **55**(5), 1769–1772 (2016)
29. Q. Zhang, X. Zhao, L. Duan, H. Shen, R. Liu, T. Hou, CrystEngComm **22**(31), 5245–5254 (2020)
30. X.H. Li, M. Antonietti, Angew. Chem. Int. Ed. Engl. **52**(17), 4572–4576 (2013)
31. C. Wu, J. Bu, J. Wang, H. Shen, Y. Cao, H. Zhang, Ind. Eng. Chem. Res. **61**(16), 5442–5452 (2022)
32. Q. Xu, B. Feng, C. Ye, Y. Fu, D.-L. Chen, F. Zhang, J. Zhang, W. Zhu, A.C.S. Appl, Mater. Interfaces **13**(13), 15168–15177 (2021)
33. S. Shubhashish, H.S. Khanna, L.A. Achola, A.S. Amin, W.S. Willis, S.L. Suib, A.C.S. Appl, Nano Mater. **4**(2), 2086–2097 (2021)
34. C.K.P. Neeli, S. Ganji, V.S.P. Ganjala, S.R.R. Kamaraju, D.R. Burri, RSC Adv. **4**(27), 14128–14135 (2014)
35. M. Gopiraman, I.M. Chung, J. Taiwan. Inst. Chem. E. **81**, 455–464 (2017)
36. J. Xu, J. Li, K. Yang, H. Li, J. Inorg. Organomet. **30**(4), 1384–1392 (2020)